NANO LETTERS

pubs.acs.org/NanoLett Letter

Molecular Orbital Insights into Plasmon-Induced Methane Photolysis

Daqiang Chen,[†] Yimin Zhang,[†] and Sheng Meng*

Cite This: *Nano Lett.* 2023, 23, 11638−11644 Read Online

ACCESS | Metrics & More | Article Recommendations | Supporting Information

ABSTRACT: As a promising way to reduce the temperature for conventional thermolysis, plasmon-induced photocatalysis has been utilized for the dehydrogenation of methane. Here we probe the microscopic dynamic mechanism for plasmon-induced methane dissociation over a tetrahedral Ag_{20} nanoparticle with molecular orbital insights using time-dependent density functional theory. We ingeniously built the relationship between the chemical bonds and molecular orbitals via Hellmann−Feynman forces. The time- and energy-resolved photocarrier analysis shows that the indirect hot hole transfer from the Ag nanoparticle to methane dominates the photoreaction at low laser intensity, due to the strong hybridization of the Ag nanoparticle and CH_4 orbitals, while indirect and direct charge transfer coexist to facilitate methane dissociation in intense laser fields. Our findings can be used to design novel methane photocatalysts and highlight the broad prospects of the molecular orbital approach for adsorbate−substrate systems.

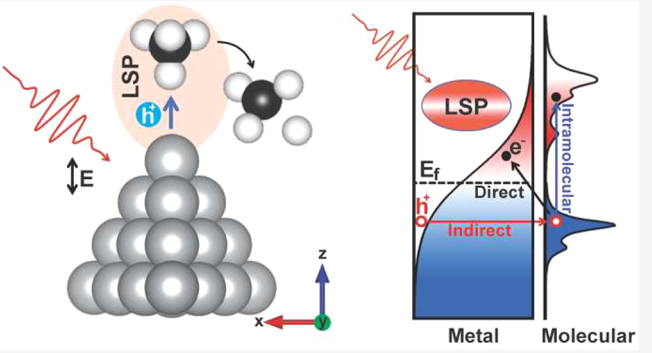

KEYWORDS: *Localized surface plasmon, methane dehydrogenation, photocarrier dynamics, molecular orbital insight, real-time time-dependent density functional theory*

Methane, as an abundant natural resource on the earth, is one of the widely used raw materials for the synthesis of high-value compounds such as CH_3OH and CH_3COOH.[1−4] Unfortunately, due to its high C−H bond strengths, negligible electron affinity, large ionization energy, and low polarizability, the activation of methane is highly challenging,[5,6] especially the activation of the first C−H bond, which is considered as one of the "Holy Grails" in catalysis.[7] Traditional approaches to activate the C−H bond require high temperature (above 800 °C) and high pressure (above 2 MPa),[8] which need consumption of plenty of fuel and result in the production of greenhouse gases. Thus, it is important to develop efficient and green approaches for methane dissociation under mild conditions.[9−11]

Plasmon-induced photolysis of CH_4 can be invoked to remedy the disadvantages of conventional thermal catalysis with the aid of plasmonic metal photocatalysts. Owing to their distinct properties such as extended lifetime, tunable resonance energy, ultrafast dynamics, and enhanced optical absorption, localized surface plasmons (LSPs) in metallic nanostructures (Au, Ag, etc.) have stimulated wide attention in chemical and solar energy conversion, especially in photocatalysis.[12−14] For plasmon-induced photocatalysis, hot carriers generated via the decay of surface plasmons can be more energetic than those generated by direct photoexcitation, which can be exploited to efficiently drive chemical reactions. Recent experiments and theoretical studies have demonstrated various types of photo-assisted chemical reactions including plasmon-induced O_2 dissociation,[15] H_2O splitting,[16] and CO_2 reduction.[17] However, due to the inactivity of CH_4 and the complex charge transfer process, plasmon-induced CH_4 photolysis is seldom systematically explored. Instead, only scattered experimental investigations have been performed, including studies involving silver−heteropolyacid−titania nanocomposites,[18] single atomic site antenna-reactor plasmonic photocatalysts,[19] and Au/ZnO porous nanosheets.[20] In the meantime, detailed investigations on the atomic processes of charge transfer in these previous works are yet missing, and consequently, the fundamental microscopic mechanism of plasmon-induced CH_4 photolysis remains elusive.

Here at the single-molecule level and femtosecond time scale, we investigate the microscopic dynamic mechanism of plasmon-induced CH_4 photolysis on plasmonic nanostructures represented by the tetrahedral Ag_{20} (Td-Ag_{20}) nanoparticle (Figure 1a). With ultrafast nonadiabatic molecular dynamics (NAMD) and carrier dynamics analysis via real-time time-dependent

Received: September 11, 2023
Revised: October 28, 2023
Accepted: October 30, 2023
Published: November 2, 2023

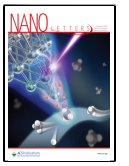

https://doi.org/10.1021/acs.nanolett.3c03467
Nano Lett. 2023, 23, 11638−11644

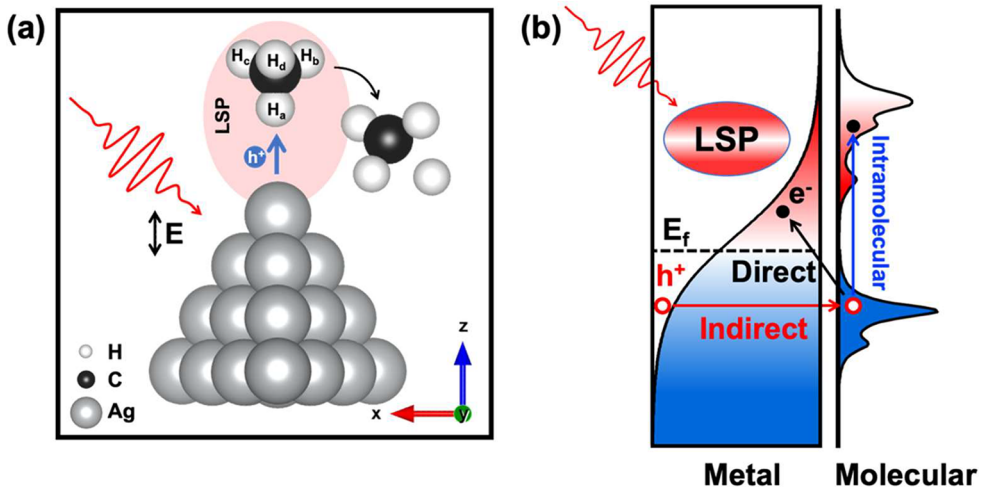

Figure 1. (a) Schematic diagram of plasmon-induced CH_4 dissociation on Td-Ag_{20} upon laser irradiation with z-directional polarization, where h^+ denotes the hole indirectly transferring from Ag to CH_4. (b) Schematic illustration of charge transfer pathways between Ag_{20} and the occupied orbitals of CH_4.

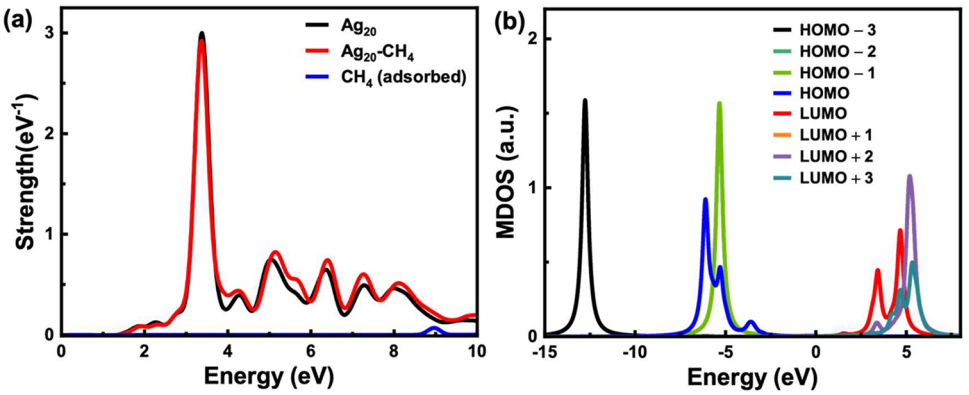

Figure 2. (a) Absorption spectra of the Td-Ag_{20} nanoparticle (black), Ag_{20}-CH_4 system (red), and isolated CH_4 after adsorption (blue). (b) Density of states projected onto every molecular orbital of isolated CH_4 for the Ag_{20}-CH_4 system. The energy is shifted to set the Fermi energy level of the Ag_{20}-CH_4 system at 0.0 eV.

density functional theory (rt-TDDFT), we quantitatively demonstrate that the photolysis originates from the synergic effects of the indirect charge transfer and the direct charge transfer. The molecular orbital analysis reveals that the strong orbital hybridization between CH_4 and Ag_{20} leads to extensive spreading of molecular orbitals, benefiting the charge transfer. The above methodology and findings provide a molecular perspective on the interaction within adsorbate−substrate systems and will facilitate the design of efficient and selective plasmonic photocatalysts.

The atomic configurations are fully relaxed by the Vienna *ab initio* Simulation Package (VASP) using density functional theory (DFT).[21,22] The ground state properties and excited state dynamics simulations are calculated using DFT[23] and rt-TDDFT[24] with the real-space code OCTOPUS.[25−27] The theory and detailed parameters are given in the Supporting Information.

The initial configuration for structure optimization is that the H atom of CH_4 locates at a distance of 3.0 Å from the vertex position of Ag_{20}, as shown in Figure 1a. For the sake of convenience, we differentiate the four H atoms of methane as H_a, H_b, H_c, and H_d, with H_a being the closest to Ag_{20}. After relaxation, the distance between Ag and H_a is reduced to 2.11 Å. Besides, compared to the initial C−H bond length (1.10 Å) for freestanding methane, the C−H_a bond length is stretched to 1.12 Å after absorption, suggesting a strong interaction between Ag_{20} and CH_4.

In order to analyze the optical response, we present the absorption spectra of the Ag_{20} nanoparticle, the optimized Ag_{20}-CH_4 system, and the isolated CH_4 after adsorption, as shown in Figure 2a. The absorption spectrum of the isolated CH_4 after adsorption shows the first peak at 8.96 eV, which is associated with the excitation from the highest occupied molecular orbital (HOMO) to the lowest unoccupied molecular orbital (LUMO). A narrow and intense peak at 3.40 eV, corresponding to the plasmonic response of Ag_{20}, is observed in the absorption spectrum, which is consistent with previous investigations.[28−31] Specifically, the plasmonic peak arises from the collective sp → sp intraband transition, and the d → sp interband transitions contribute to the spectrum at the higher energy range.[31] Compared with Ag_{20}, the absorption spectrum of Ag_{20}-CH_4 exhibits the same plasmon resonance feature at 3.40 eV but shows significant enhancement at the higher energy range.

To address the electronic structure of the adsorption system, we present the density of states (DOS) projected onto every molecular orbital (MDOS) of isolated CH_4 for the Ag_{20}-CH_4 system in Figure 2b. The MDOS of the HOMO−3 and the two-fold degenerate orbitals (HOMO−2 and HOMO−1) show no

https://doi.org/10.1021/acs.nanolett.3c03467
Nano Lett. 2023, 23, 11638−11644

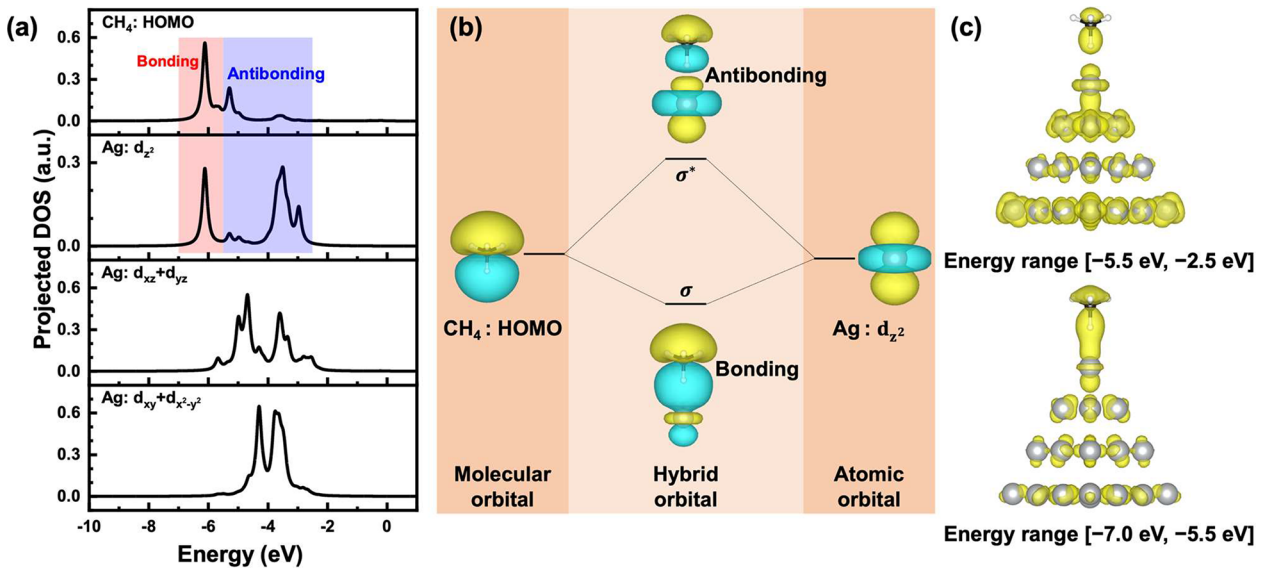

Figure 3. (a) Density of states for the Ag_{20}-CH_4 system projected to the HOMO orbitals of CH_4 (top panel), and the d_{z^2} (second panel), $d_{xz} + d_{yz}$ (third panel), and $d_{xy} + d_{x^2-y^2}$ (bottom panel) orbitals of the top Ag atom. (b) Formation diagram of the bonding and antibonding states and the (c) corresponding distribution of charge density after the interaction between the HOMO orbitals of CH_4 and the Ag d_{z^2} orbitals. Here, the isosurface value is 0.04 e/Å^3.

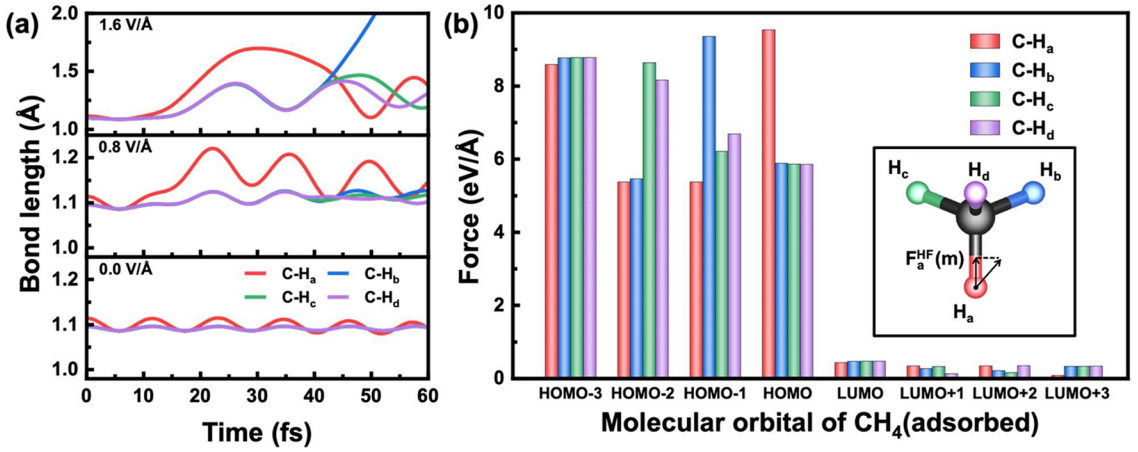

Figure 4. (a) Time-evolved C−H bond length in the Ag_{20}-CH_4 system under laser radiation with field strength E_{max} = 0.0, 0.8, and 1.6 V/Å. (b) Hellmann−Feynman force $F_x^{HF}(m)$ along the C−H_x (x = a, b, c, d) bond. Here, the index m denotes the molecular orbital order for the adsorbed CH_4 molecule, that is, HOMO−3, HOMO−2, HOMO−1, HOMO, LUMO, LUMO+1, LUMO+2, and LUMO+3. The inset denotes the decomposition of the HF force along the bond direction.

splitting, indicating that these orbitals have minimal interaction with Ag_{20} upon adsorption. Conversely, the strong interaction between the HOMO and Ag_{20} leads to a wide distribution of MDOS over many KS orbitals, with two main peaks at −6.10 eV and −5.30 eV, and one weak peak at −3.60 eV. The emergence of new hybrid orbitals can qualify the adsorption mechanism in the Ag_{20}-CH_4 system as chemisorption.[32]

The orbital hybridization can be understood in terms of the well-known d-band model: the coupling between the HOMO and the narrow distribution of d-states gives rise to the formation of separated bonding and antibonding states.[33−35] In Figure 3a, the projected DOS reveals that the d_{z^2} orbital of the Ag atom hybridizes strongly with the HOMO of CH_4 compared to the d_{xz}, d_{yz}, d_{xy}, and $d_{x^2-y^2}$ orbitals. As illustrated in Figure 3b, due to the symmetry matching,[36] the HOMO overlaps with the Ag d_{z^2} orbital to form a σ bonding state at low energy level and forms a σ^* antibonding state at high energy level. For a more obvious demonstration of the hybridization between the HOMO of CH_4 and the d_{z^2} orbitals of Ag, the charge density distributions of the hybrid orbitals in Ag_{20}-CH_4 at different energy ranges are shown in Figure 3c, which also exhibits the signatures of the bonding and antibonding states. The hybridization not only enhances the absorption spectrum corresponding to the d → sp interband transition but also broadens the molecular orbitals, facilitating the charge transfer between CH_4 and Ag_{20}.[37]

In order to explore the effect of Ag_{20} on methane dehydrogenation, we further investigated the dynamic response of Ag_{20}-CH_4 under laser radiation with different maximum field strengths E_{max}. The frequency ω of the applied laser pulse is set to be identical to the plasmon resonance frequency of Ag_{20}, i.e., $\hbar\omega$ = 3.40 eV. Figure 4a illustrates the time-resolved C−H bond lengths of CH_4 in the NAMD simulations. Without laser irradiation, the C−H bond lengths show stable oscillation with an amplitude of less than 0.03 Å, indicating that methane

https://doi.org/10.1021/acs.nanolett.3c03467
Nano Lett. 2023, 23, 11638−11644

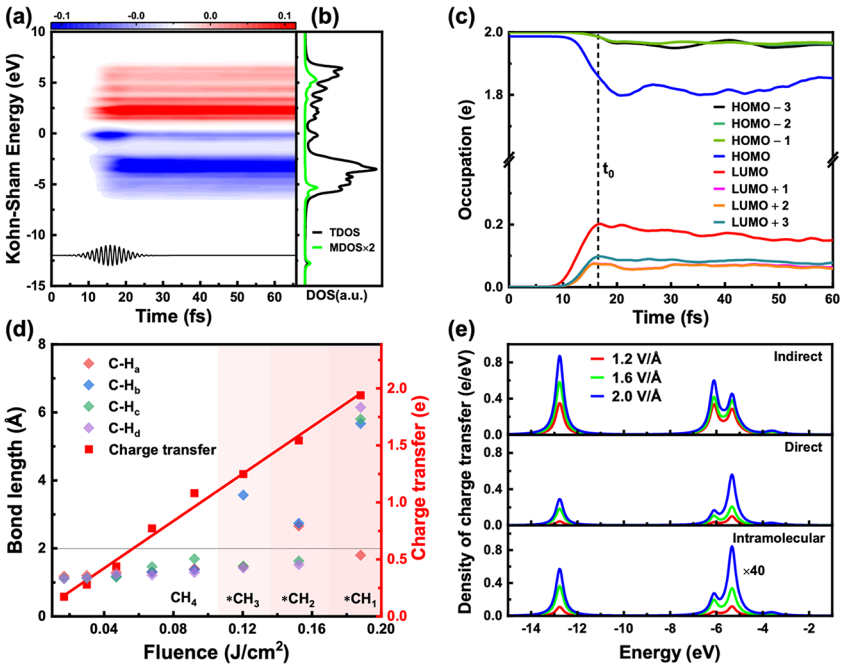

Figure 5. (a) The time-dependent occupations of the Kohn−Sham states in Ag_{20}-CH_4 under laser radiation, where the black curve denotes the laser pulse. (b) Total density of states (TDOS) and density of states projected onto all molecular orbitals of the adsorbed CH_4 (MDOS) for the Ag_{20}-CH_4 system. For a better view, the value of MDOS has been zoomed in by 2 times (×2). (c) Time-dependent evolution of the occupation numbers for the molecular orbitals of adsorbed CH_4 in the Ag_{20}-CH_4 system. The occupation numbers for the LUMO ∼ LUMO+3 reach their maximum at t_0 = 15.8 fs, indicated by the black vertical dashed line. (d) Maximum of the C−H_x (x = a, b, c, d) bond length and charge transfer involving the occupied molecular orbitals at different laser fluences. Here, the diamond symbols at each laser fluence represent the maximum of the four C−H bond lengths of Ag_{20}-CH_4 within 40 fs after light irradiation. The black dashed line indicates that the C−H bond is broken at 2.0 Å. The red square symbols are the loss of charge for the occupied orbitals (summed over the HOMO−3, HOMO−2, HOMO−1, and HOMO of the adsorbed CH_4) in the Ag_{20}-CH_4 system after light radiation, and the solid red line is a linear fit of the charge transfer against the laser fluence. (e) Density of photoinduced charge transfer through three channels, i.e., indirect, direct, and intramolecular charge transfer from the occupied orbitals of CH_4 to Ag_{20}. For a better view, the value of intramolecular charge transfer has been zoomed in by 40 times (×40).

dehydrogenation does not occur directly after adsorption on the Ag_{20} nanoparticle. When E_{max} is 0.8 V/Å, the C−H bond lengths increase significantly with laser radiation and then exhibit periodic oscillations. In particular, when E_{max} reaches 1.6 V/Å, the C−H bonds oscillate violently and CH_4 splits into a methyl radical (CH_3) and hydrogen atom at time t = 50.0 fs. It is also evident that the plasmon resonance modulates the vibrational phonon modes of CH_4. First, the symmetric stretching mode of CH_4 is enhanced. Subsequently, the oscillation phases of the C−H bond lengths become asynchronous, indicating the generation of the antisymmetric stretching mode. In other words, the plasmon enhances the molecular vibrations and induces the intramolecular vibrational energy redistribution.[38] In contrast, the C−H bonds of freestanding CH_4 remain unbroken even at an E_{max} of 1.6 V/Å (Figure S2), as its primary absorption peak lies at 8.96 eV, much larger than 3.4 eV. These findings suggest that methane dehydrogenation is induced by the localized plasmon excitation of the Ag nanoparticle.

To give a straightforward relationship between bond lengths and molecular orbitals, we calculated the Hellmann−Feynman (HF) force acting on the H atoms for each molecular orbital (see Supporting Information for details). As shown in Figure 4b, the positive $F_x^{HF}(m)$ indicates that each molecular orbital tends to shorten the C−H bond lengths. The $F_x^{HF}(m)$ of the occupied molecular orbitals (m = HOMO−3 ∼ HOMO) is much larger than that for the unoccupied orbitals (m = LUMO ∼ LUMO +3), which is determined by their spatial distribution. Consequently, the stretching of the C−H bond is dominated by the reduction of the number of electrons in the occupied orbitals.

To understand the underlying microscopic mechanism of methane dehydrogenation induced by localized plasmon excitation, we further analyze the carrier dynamics as shown in Figure 5. Figure 5a shows the time- and energy-resolved photocarrier distribution, in which the excited electrons and holes exhibit a fast response to the laser pulse in the energy range around the Fermi level due to the strong oscillation in the charge density near the Ag_{20} surface.[39] Besides, it can be seen that the electrons can be excited from the relatively low energy region to the high energy levels, which indicated the existence of the plasmon decay.[40,41] Combined with Figures 5a and 5b, the hot carrier distribution overlaps with the MDOS, suggesting a possible charge transfer between Ag_{20} and CH_4.

With the intent of providing a clear depiction of photocarrier dynamics, Figure 5c illustrates the time-resolved occupation numbers located on the methane orbitals for the Ag_{20}-CH_4 system. Under laser irradiation, the populations of LUMO ∼ LUMO+3 increase until the laser intensity reaches E_{max} at t_0 = 15.8 fs. Moreover, the occupations of the unoccupied molecular orbitals (LUMO ∼ LUMO+3) are greater than the decrease in the occupations of the occupied molecular orbitals (HOMO−3 ∼ HOMO), as marked by the dashed black line in Figure 5c. These findings suggest that the electrons on LUMO ∼ LUMO +3 are donated by photoexcited Ag_{20}. In contrast, the electrons on the HOMO continue to decrease during $t > t_0$, indicating that

https://doi.org/10.1021/acs.nanolett.3c03467
Nano Lett. 2023, 23, 11638−11644

the process is dominated by charge transfer between methane and Ag_{20}.

In plasmon-induced photocatalysis, charge transfer between the substrate and molecule can initiate the chemical conversion of the molecule.[13,17,42] Combining the Hellmann−Feynman force analysis with atomic and electronic dynamical responses, methane dehydrogenation is induced by the charge transfer involving the occupied molecular orbitals. As illustrated in Figure 1b, the transfer pathways can be classified into three categories. (a) Indirect charge transfer: Plasmon resonances in nanostructures can be damped nonradiatively through Landau damping to generate hot carriers which can be transferred to molecular orbitals to induce chemical reactions, and this process is called indirect charge transfer.[12,43−47] Notably, the indirect charge transfer here is indirect hot hole transfer from the Ag nanoparticle to the occupied orbitals of CH_4. (b) Direct charge transfer: Nonradiative plasmon decay can directly excite electrons from molecules to metals, which is known as direct charge transfer.[47] (c) Intramolecular charge transfer: This term refers to the excitation of electrons from occupied molecular orbitals to unoccupied molecular orbitals.[48]

In Figure 5d, the C−H bond lengths and charge transfer involving the occupied molecular orbitals at various laser fluences are illustrated. The charge transfer ΔQ exhibits a significantly linear feature with the laser fluence, which has also been observed in plasmon-induced water splitting on gold nanoparticles.[16] Below the critical fluence of 120 mJ/cm^2 (E_{max} = 1.6 V/Å), the C−H bond becomes weaker as the transferred charge increases, exhibiting a stretching of the C−H bond. Once the laser fluence exceeds the critical value, apart from the formation of methyl (CH_3), the C−H bond in CH_4 will break continuously with the increase of the transfer charge to form methylene (CH_2) and methylidyne (CH).

Figure 5e illustrates the densities of the three types of charge transfer from the occupied molecular orbitals over a wide energy range. The detailed methodology is available in the Supporting Information. Several observations can be obtained through the analysis below:

(i) Indirect charge transfer (ICT). The ICT shows the biggest density of charge transfer at different field strengths, which indicates that ICT is the dominant charge transfer pathway for plasmon-induced methane dissociation. This can be attributed to the continuous distribution of holes under the Fermi level and the broad hybridization between CH_4 and Ag_{20}. This conclusion is consistent with many experimental studies that have shown that C−H bond cleavage is induced by hot hole transfer.[18]

(ii) Direct charge transfer (DCT). At low laser intensity, the density of DCT is about ten times smaller than that for ICT, indicating that DCT plays a minor role in the reaction process. At large laser fluence 188 mJ/cm^2 (E_{max} = 2.0 V/Å), DCT predominantly occurs in the molecular orbitals located near −5.34 eV, while ICT remains dominant in other energy ranges. Besides, the DOS in Figure 5b reveals an energy gap of approximately $2\hbar\omega$ = 6.80 eV between the main peak of the MDOS (at −5.34 eV) and the energy level of the lowest unoccupied KS orbital (at 1.47 eV), implying that DCT is a double-photon absorption process. Moreover, a recent study has highlighted significant double-photon transitions during the plasmon decay in the Ag_{20} nanoparticle.[28]

(iii) Intramolecular charge transfer. The efficiency of intramolecular charge transfer is 2 orders of magnitude weaker than that of DCT and ICT for two reasons. First, the MDOS in Figure 5b indicates that the excitation between molecular orbitals requires absorption of three or even more photons with energy of $\hbar\omega$ = 3.40 eV. However, the triple-photon transition is very weak in the nonradiative decay of the plasmon in the Ag_{20} nanoparticle.[28] Second, the contribution of the CH_4 molecule to the TDOS is much smaller than that for the Ag substrate.

In conclusion, taking Ag_{20}-CH_4 as a prototypic model, we have presented a novel methodology and analysis based on the molecular orbital approach to describe the ultrafast structure and photocarrier dynamics in the plasmon-induced methane photolysis within the framework of DFT and TDDFT. The time-resolved photocarrier dynamics confirms that indirect hole transfer dominates the methane dehydrogenation due to the strong coupling between the Ag d_{z^2} orbital and the HOMO orbital of CH_4 in the Ag_{20}-CH_4 system at low laser intensity, while the direct charge transfer synergistically stimulates the reaction under high-intensity laser pulses. The present findings provide a novel insight into the interaction between the substrate and adsorbate from the view of molecular orbitals, which can be widely applied to investigate the dynamic charge transfer processes between adsorbates and substrates, benefiting the design of highly efficient plasmon-induced photocatalysts.

■ ASSOCIATED CONTENT

Data Availability Statement

The data that support the findings of this study are available from the corresponding author upon reasonable request.

Supporting Information

The Supporting Information is available free of charge at https://pubs.acs.org/doi/10.1021/acs.nanolett.3c03467.

Details on density functional theory and real-time time-dependent density functional theory calculations; Formulas for time- and energy-resolved carrier distribution, density of states projected onto molecular orbitals, time-dependent evolution of occupation number for molecular orbitals, energy-resolved charge transfer between substrate and molecule, and Hellmann−Feynman force of molecular orbitals; Time-resolved C−H bond lengths of freestanding CH_4; Time-resolved evolutions of charge transfer; Discussion about the size effect of Ag nanoparticle. (PDF)

■ AUTHOR INFORMATION

Corresponding Author

Sheng Meng − *Beijing National Laboratory for Condensed Matter Physics and Institute of Physics, Chinese Academy of Sciences, Beijing 100190, P. R. China; School of Physical Sciences, University of Chinese Academy of Sciences, Beijing 100049, P. R. China; Songshan Lake Materials Laboratory, Dongguan, Guangdong 523808, P. R. China;* orcid.org/0000-0002-1553-1432; Email: smeng@iphy.ac.cn

Authors

Daqiang Chen − *Beijing National Laboratory for Condensed Matter Physics and Institute of Physics, Chinese Academy of Sciences, Beijing 100190, P. R. China; School of Physical Sciences, University of Chinese Academy of Sciences, Beijing 100049, P. R. China*

Yimin Zhang − *Key Laboratory of Material Physics, Ministry of Education, School of Physics and Microelectronics, Zhengzhou University, Zhengzhou 450001, P. R. China*

Complete contact information is available at: https://pubs.acs.org/10.1021/acs.nanolett.3c03467

Author Contributions

†D.C. and Y.Z. contributed equally. S.M. and Y.Z. designed and directed the project. D.C. proposed the methodologies, developed the analysis codes, and carried out the simulations. All authors contributed to the discussions and analyses of the data, and approved the final version.

Notes

The authors declare no competing financial interest.

■ ACKNOWLEDGMENTS

We acknowledge financial support from the Ministry of Science and Technology (No. 2021YFA1400201), National Natural Science Foundation of China (No. 12025407, No.12304351 and No. 11934004), and Chinese Academy of Sciences (No. YSBR047 and No. XDB330301).

■ REFERENCES

(1) Luo, L.; Fu, L.; Liu, H.; Xu, Y.; Xing, J.; Chang, C.-R.; Yang, D.-Y.; Tang, J. Synergy of Pd atoms and oxygen vacancies on In2O3 for methane conversion under visible light. *Nat. Commun.* **2022**, *13*, 2930.

(2) Sushkevich, V. L.; Palagin, D.; Ranocchiari, M.; Van Bokhoven, J. A. Selective anaerobic oxidation of methane enables direct synthesis of methanol. *Science* **2017**, *356*, 523−527.

(3) Schwach, P.; Pan, X.; Bao, X. Direct conversion of methane to value-added chemicals over heterogeneous catalysts: challenges and prospects. *Chem. Rev.* **2017**, *117*, 8497−8520.

(4) Meng, X.; Cui, X.; Rajan, N. P.; Yu, L.; Deng, D.; Bao, X. Direct methane conversion under mild condition by thermo-, electro-, or photocatalysis. *Chem.* **2019**, *5*, 2296−2325.

(5) Jin, Z.; Wang, L.; Zuidema, E.; Mondal, K.; Zhang, M.; Zhang, J.; Wang, C.; Meng, X.; Yang, H.; Mesters, C. Hydrophobic zeolite modification for in situ peroxide formation in methane oxidation to methanol. *Science* **2020**, *367*, 193−197.

(6) Larkins, F.; Khan, A. Pyrolysis of methane to higher hydrocarbons: A thermodynamic study. *Aust. J. Chem.* **1989**, *42*, 1655−1670.

(7) Tomkins, P.; Ranocchiari, M.; van Bokhoven, J. A. Direct conversion of methane to methanol under mild conditions over Cu-zeolites and beyond. *Accounts of Chemical Research* **2017**, *50*, 418−425.

(8) Hu, D.; Ordomsky, V. V.; Khodakov, A. Y. Major routes in the photocatalytic methane conversion into chemicals and fuels under mild conditions. *Applied Catalysis B: Environmental* **2021**, *286*, 119913.

(9) Li, X.; Wang, C.; Tang, J. Methane transformation by photocatalysis. *Nature Reviews Materials* **2022**, *7*, 617−632.

(10) Xie, J.; Jin, R.; Li, A.; Bi, Y.; Ruan, Q.; Deng, Y.; Zhang, Y.; Yao, S.; Sankar, G.; Ma, D. Highly selective oxidation of methane to methanol at ambient conditions by titanium dioxide-supported iron species. *Nature Catalysis* **2018**, *1*, 889−896.

(11) Song, H.; Meng, X.; Wang, Z.-j.; Wang, Z.; Chen, H.; Weng, Y.; Ichihara, F.; Oshikiri, M.; Kako, T.; Ye, J. Visible-light-mediated methane activation for steam methane reforming under mild conditions: a case study of Rh/TiO2 catalysts. *ACS Catal.* **2018**, *8*, 7556−7565.

(12) Brongersma, M. L.; Halas, N. J.; Nordlander, P. Plasmon-induced hot carrier science and technology. *Nature Nanotechnol.* **2015**, *10*, 25−34.

(13) Linic, S.; Aslam, U.; Boerigter, C.; Morabito, M. Photochemical transformations on plasmonic metal nanoparticles. *Nature materials* **2015**, *14*, 567−576.

(14) Xin, Y.; Yu, K.; Zhang, L.; Yang, Y.; Yuan, H.; Li, H.; Wang, L.; Zeng, J. Copper-Based Plasmonic Catalysis: Recent Advances and Future Perspectives. *Adv. Mater.* **2021**, *33*, 2008145.

(15) Christopher, P.; Xin, H.; Linic, S. Visible-light-enhanced catalytic oxidation reactions on plasmonic silver nanostructures. *Nature Chem.* **2011**, *3*, 467−472.

(16) Yan, L.; Wang, F.; Meng, S. Quantum mode selectivity of plasmon-induced water splitting on gold nanoparticles. *ACS Nano* **2016**, *10*, 5452−5458.

(17) Zhang, Y.; Yan, L.; Guan, M.; Chen, D.; Xu, Z.; Guo, H.; Hu, S.; Zhang, S.; Liu, X.; Guo, Z. Indirect to Direct Charge Transfer Transition in Plasmon-Enabled CO2 Photoreduction. *Advanced Science* **2022**, *9*, 2102978.

(18) Yu, X.; Zholobenko, V. L.; Moldovan, S.; Hu, D.; Wu, D.; Ordomsky, V. V.; Khodakov, A. Y. Stoichiometric methane conversion to ethane using photochemical looping at ambient temperature. *Nature Energy* **2020**, *5*, 511−519.

(19) Zhou, L.; Martirez, J. M. P.; Finzel, J.; Zhang, C.; Swearer, D. F.; Tian, S.; Robatjazi, H.; Lou, M.; Dong, L.; Henderson, L. Light-driven methane dry reforming with single atomic site antenna-reactor plasmonic photocatalysts. *Nature Energy* **2020**, *5*, 61−70.

(20) Meng, L.; Chen, Z.; Ma, Z.; He, S.; Hou, Y.; Li, H.-H.; Yuan, R.; Huang, X.-H.; Wang, X.; Wang, X. Gold plasmon-induced photocatalytic dehydrogenative coupling of methane to ethane on polar oxide surfaces. *Energy Environ. Sci.* **2018**, *11*, 294−298.

(21) Kresse, G.; Joubert, D. From ultrasoft pseudopotentials to the projector augmented-wave method. *Physical review b* **1999**, *59*, 1758.

(22) Kresse, G.; Furthmüller, J. Efficiency of ab-initio total energy calculations for metals and semiconductors using a plane-wave basis set. *Computational materials science* **1996**, *6*, 15−50.

(23) Kohn, W.; Sham, L. J. Self-consistent equations including exchange and correlation effects. *Physical review* **1965**, *140*, A1133.

(24) Runge, E.; Gross, E. K. Density-functional theory for time-dependent systems. *Physical review letters* **1984**, *52*, 997.

(25) Tancogne-Dejean, N.; Oliveira, M. J.; Andrade, X.; Appel, H.; Borca, C. H.; Le Breton, G.; Buchholz, F.; Castro, A.; Corni, S.; Correa, A. A. Octopus, a computational framework for exploring light-driven phenomena and quantum dynamics in extended and finite systems. *J. Chem. Phys.* **2020**, *152*, 124119.

(26) Castro, A.; Appel, H.; Oliveira, M.; Rozzi, C. A.; Andrade, X.; Lorenzen, F.; Marques, M. A.; Gross, E.; Rubio, A. Octopus: a tool for the application of time-dependent density functional theory. *physica status solidi (b)* **2006**, *243*, 2465−2488.

(27) Marques, M. A.; Castro, A.; Bertsch, G. F.; Rubio, A. octopus: a first-principles tool for excited electron-ion dynamics. *Comput. Phys. Commun.* **2003**, *151*, 60−78.

(28) Kuda-Singappulige, G. U.; Aikens, C. M. Excited-state absorption in silver nanoclusters. *J. Phys. Chem. C* **2021**, *125*, 24996−25006.

(29) Guidez, E. B.; Aikens, C. M. Quantum mechanical origin of the plasmon: from molecular systems to nanoparticles. *Nanoscale* **2014**, *6*, 11512−11527.

(30) Gieseking, R. L.; Ratner, M. A.; Schatz, G. C. Semiempirical modeling of Ag nanoclusters: New parameters for optical property studies enable determination of double excitation contributions to plasmonic excitation. *J. Phys. Chem. A* **2016**, *120*, 4542−4549.

(31) Aikens, C. M.; Li, S.; Schatz, G. C. From discrete electronic states to plasmons: TDDFT optical absorption properties of Ag n (n= 10, 20, 35, 56, 84, 120) tetrahedral clusters. *J. Phys. Chem. C* **2008**, *112*, 11272−11279.

(32) Müller, K.; Seitsonen, A. P.; Brugger, T.; Westover, J.; Greber, T.; Jung, T.; Kara, A. Electronic structure of an organic/metal interface: Pentacene/Cu (110). *J. Phys. Chem. C* **2012**, *116*, 23465−23471.

(33) Lang, N.; Williams, A. Theory of atomic chemisorption on simple metals. *Phys. Rev. B* **1978**, *18*, 616.

(34) Nilsson, A.; Pettersson, L.; Hammer, B.; Bligaard, T.; Christensen, C. H.; Nørskov, J. K. The electronic structure effect in heterogeneous catalysis. *Catal. Lett.* **2005**, *100*, 111−114.

(35) Pettersson, L. G. M.; Nilsson, A. A molecular perspective on the d-band model: synergy between experiment and theory. *Top. Catal.* **2014**, *57*, 2−13.
(36) Qiao, W.; Yan, S.; Jin, D.; Xu, X.; Mi, W.; Wang, D. Vertical-orbital band center as an activity descriptor for hydrogen evolution reaction on single-atom-anchored 2D catalysts. *J. Phys.: Condens. Matter* **2021**, *33*, 245201.
(37) Chen, C.; Yang, S.; Su, G.; Li, J.; Ren, J.-C.; Liu, W. Conductance Switching in Molecular Self-Assembled Monolayers for Application of Data Storage. *J. Phys. Chem. C* **2021**, *125*, 1069−1074.
(38) Killelea, D. R.; Campbell, V. L.; Shuman, N. S.; Utz, A. L. Bond-selective control of a heterogeneously catalyzed reaction. *Science* **2008**, *319*, 790−793.
(39) Townsend, E.; Bryant, G. W. Plasmonic properties of metallic nanoparticles: The effects of size quantization. *Nano Lett.* **2012**, *12*, 429−434.
(40) Townsend, E.; Bryant, G. W. Which resonances in small metallic nanoparticles are plasmonic? *Journal of Optics* **2014**, *16*, 114022.
(41) Ma, J.; Wang, Z.; Wang, L.-W. Interplay between plasmon and single-particle excitations in a metal nanocluster. *Nat. Commun.* **2015**, *6*, 10107.
(42) Linic, S.; Christopher, P.; Ingram, D. B. Plasmonic-metal nanostructures for efficient conversion of solar to chemical energy. *Nature materials* **2011**, *10*, 911−921.
(43) Li, X.; Xiao, D.; Zhang, Z. Landau damping of quantum plasmons in metal nanostructures. *New J. Phys.* **2013**, *15*, 023011.
(44) Manjavacas, A.; Liu, J. G.; Kulkarni, V.; Nordlander, P. Plasmon-induced hot carriers in metallic nanoparticles. *ACS Nano* **2014**, *8*, 7630−7638.
(45) Jin, R.; Charles Cao, Y.; Hao, E.; Métraux, G. S.; Schatz, G. C.; Mirkin, C. A. Controlling anisotropic nanoparticle growth through plasmon excitation. *Nature* **2003**, *425*, 487−490.
(46) Wu, X.; Thrall, E. S.; Liu, H.; Steigerwald, M.; Brus, L. Plasmon induced photovoltage and charge separation in citrate-stabilized gold nanoparticles. *J. Phys. Chem. C* **2010**, *114*, 12896−12899.
(47) Thrall, E. S.; Preska Steinberg, A.; Wu, X.; Brus, L. E. The role of photon energy and semiconductor substrate in the plasmon-mediated photooxidation of citrate by silver nanoparticles. *J. Phys. Chem. C* **2013**, *117*, 26238−26247.
(48) Kazuma, E.; Jung, J.; Ueba, H.; Trenary, M.; Kim, Y. Real-space and real-time observation of a plasmon-induced chemical reaction of a single molecule. *Science* **2018**, *360*, 521−526.

https://doi.org/10.1021/acs.nanolett.3c03467
Nano Lett. 2023, 23, 11638−11644